Decoding Natural Grasping Behaviors: Insights Into MRCP Source Features and Coupling Dynamics

Leying Deng, Baoguo Xu, *Member, IEEE*, Zelin Gao, Minmin Miao, Cong Hu, and Aiguo Song, *Senior Member, IEEE*

***Abstract*— The effective decoding of natural grasping behaviors is crucial for the natural control of neural prosthetics. This study aims to investigate the decoding performance of movement-related cortical potential (MRCP) source features between complex grasping actions and explore the temporal and frequency differences in inter-muscular and cortical-muscular coupling strength during movement. Based on the human grasping taxonomy and their frequency, five natural grasping motions—medium wrap, adducted thumb, adduction grip, tip pinch, and writing tripod—were chosen. We collected 64-channel electroencephalogram (EEG) and 5-channel surface electromyogram (sEMG) data from 17 healthy participants, and projected six EEG frequency bands into source space for further analysis. Results from multi-classification and binary classification demonstrated that MRCP source features could not only distinguish between power grasp and precision grasp, but also detect subtle action differences such as thumb adduction and abduction during the execution phase. Besides, we found that during natural reach-and-grasp movement, the coupling strength from cortical to muscle is lower than that from muscle to cortical, except in the hold phase of γ frequency band. Furthermore, a 12-Hz peak of inter-muscular coupling strength was found in movement execution, which might be related to movement planning and execution. We believe that this research will enhance our comprehension of the control and feedback mechanisms of human hand grasping and contributes to a natural and intuitive control for brain-computer interface.**

***Index Terms*— Natural grasp decoding, movement-related cortical potential, EEG source imaging, inter-muscular coupling, cortical-muscular coupling.**

I. Introduction

IN MODERN life, many people suffer from neuromuscular disorders such as stroke and spinal cord injury (SCI). These conditions often result in individuals being conscious but unable to control their bodies, making communication and interaction with the outside world challenging. Hand function is one of the most common and crucial elements of daily life, involving the coordination and integration of various sensory and motor systems. For individuals who suffer from limb paralysis or other hand impairments, the restoration of hand functionality is vital for raising their life quality and promoting social engagement.

A brain-computer interface (BCI) is a control and communication system that enables individuals to directly interact with the outside world using their brains, bypassing the peripheral nervous systems and muscles [1]. In traditional BCI systems, users control robots or devices by imagining or performing movements from several body parts [2], [3]. However, for BCI users, such control strategy is unnatural and counterintuitive, and requires extensive training to achieve satisfactory control performance.

Recently, researchers have discovered that during the execution of cued or voluntary movements, the human engages cognitive resources in the brain associated with movement, resulting in a negative low-frequency potential acknowledged as movement-related cortical potential (MRCP) [4]. Generally, MRCP shows up as a negative amplitude shift during movement preparation stage, peaking at the movement onset and then rebounding positively. It is significant to highlight

Manuscript received 3 July 2023; revised 21 September 2023 and 5 November 2023; accepted 8 December 2023. Date of publication 13 December 2023; date of current version 20 December 2023. This work was supported in part by the National Key Research and Development Program of China under Grant 2022YFC2405602; in part by the Natural Science Foundation of Jiangsu Province under Grant BK20221464; in part by the Key Research and Development Program of Jiangsu Province under Grant BE2022363; in part by the Basic Research Project of Leading Technology of Jiangsu Province under Grant BK20192004; in part by the National Natural Science Foundation of China under Grant 92148205, Grant 62173088, and Grant 62173089; in part by the Guangxi Key Laboratory of Automatic Detecting Technology and Instruments under Grant YQ22207; and in part by the Chinese Institute of Electronic (CIE)-Tencent Robotics X Rhino-Bird Focused Research Program. *(Corresponding author: Baoguo Xu.)*

This work involved human subjects or animals in its research. Approval of all ethical and experimental procedures and protocols was granted by the Ethical Committee of Southeast University under Application No. 2020-SR-362.

Leying Deng, Baoguo Xu, Zelin Gao, and Aiguo Song are with the State Key Laboratory of Digital Medical Engineering, the Jiangsu Key Laboratory of Remote Measurement and Control, and the School of Instrument Science and Engineering, Southeast University, Nanjing 210096, China (e-mail: 15695299118@163.com; xubaoguo@seu.edu.cn; 220223274@seu.edu.cn; a.g.song@seu.edu.cn).

Minmin Miao is with the School of Information Engineering, Huzhou University, Huzhou 313000, China (e-mail: 02764@zjhu.edu.cn).

Cong Hu is with the Guangxi Key Laboratory of Automatic Detecting Technology and Instruments, Guilin University of Electronic Technology, Guilin 541004, China (e-mail: yiqi@guet.edu.cn).

Digital Object Identifier 10.1109/TNSRE.2023.3342426

that MRCP can be observed in both executed movements and imagined movements and contains information regarding movement types and parameters [5], [6]. As a result, many researchers have started investigating the decoding of MRCP in order to obtain natural and fine control in BCI systems. [7], [8], [9], [10], [11], [12]. Schwarz et al. effectively decoded three natural grasping actions (palmar grasp, pincer grasp, and lateral grasp) as well as a no-movement condition using MRCP and explored significant differences among the four conditions [13]. Wang et al. found that the event-related desynchronization (ERD) and MRCP features prior to movement initiation contain significant discriminative information, which can be effectively identified using a combination method of discriminative canonical pattern matching and common spatial patterns (CSP) [14]. Moreover, incorporating MRCP and ERS/D oscillations, Wang et al. introduced an innovative deep learning model, with six-class classification accuracy for unimanual and bimanual movements reaching 80.3% [15].

However, due to the limited spatial resolution of EEG, the decoding performance for unimanual movements is still not ideal. To address this issue, one feasible solution is to project EEG from the scalp to the cortical surface [16]. Srrisrisawang and Müller-Putz compared the decoding performance of hand trajectories between using template head models and participant-specific head models, and found no significant statistical differences [17]. Handiru et al. employed dipole source features to classify arm movements and achieved an average accuracy of 71% for four categories, which was more than 10% higher than the classification accuracy obtained using the most advanced sensor features [18]. Hou et al. combined source features with convolutional neural networks and achieved a 14.4% improvement over state-of-the-art motor imagery (MI) classification approaches [19]. Kobler et al. found that MRCP carried the initiation and direction information of arm movements, which are represented in two different cortical networks [20]. Li et al. demonstrated that EEG signals obtained from the source domain could improve the MRCP detection rather than those in the sensor domain [21].

Furthermore, we must emphasize that although improving decoding accuracy is crucial, studying the control and response mechanisms of the neuro-muscular system during movement should never be disregarded. Previous research has revealed that the motor neural system conveys movement control information via neural oscillations, resulting in synchronous oscillatory activities of motor units [22]. This oscillation is bidirectional, meaning it not only conveys commands from the cortical areas to the muscles (downward transmission) but also involves feedback from the muscles to the cortical areas (upward transmission) [23]. Omlor et al. discovered that the significant coherence of static force was limited to the β frequency band, whereas under dynamic force, the cortical-spinal oscillatory patterns of the somatomotor system shifted to higher frequencies, primarily in the γ band, to quickly integrate the visual and proprioceptive information required for generating relevant motor commands [24]. Zhu et al. discovered significant statistical coupling distinctions among various grasping actions within the β frequency band during the execution phase and notable differences within the γ frequency band during the preparation phase [25]. Zhou et al. discovered that movement observation (MO) and movement execution (ME) exhibited contralateral dominance in spatial coherence between the cortex and muscles, whereas MI displayed ipsilateral dominance [26].

In our previous studies, we have conducted research on the decoding of movement types and parameters for natural reach-and-grasps. We successfully classified the MRCP of natural grasp types under different movement parameters as well as movement parameters under each grasp type [27], [28], and explored the differences in cortical activation patterns and brain network structures among six natural grasping tasks [29]. According to human grasp taxonomy, each type of grasping actions can be accurately categorized based on the power and precision employed during execution [29], [30]. However, in the majority of studies, including our earlier research, the aspect of grasp taxonomy has not been effectively considered. Additionally, the investigation of EEG source imaging and the coupling relationship between the cortical signals and muscles may help with the precise and natural control of rehabilitation robots, especially in the field of neural prosthetics. To the best of our knowledge, however, there is limited academic research focused on MRCP source features and the coupling dynamics specific to natural grasp types.

Hence, in this study, we chose five natural grasping actions based on human grasp taxonomy [31] and action frequency [32] to conduct decoding research, which included medium wrap (MW), adducted thumb (AT), adduction grip (AG), tip pinch (TP), and writing tripod (WT). Our aim was to investigate the possibility of decoding complex action types using source features of MRCP and to explore the temporal changes and frequency band differences of inter-muscular coupling and cortical-muscular coupling strength during the natural grasping process. We believe our work will lead to a more thorough understanding of the brain's control mechanisms for grasping actions.

II. Methods

A. Participants

The experiment received approvals from the Ethics Committee of Southeast University (2020-SR-362). A total of 17 healthy participants (aged 22 to 25 years, eight males) were recruited. All participants were right-handed, with no history of neurological or muscle disorders, and had a normal or corrected-to-normal vision. For the convenience of the following discussion, these 17 participants were individually labeled as S1-S17. Before the experiment, each participant was informed about the purpose and procedures of the study and signed the informed consent.

B. Experimental Paradigm

The experiment was conducted in a quiet and electromagnetically shielded room to minimize the influence of environmental factors. The experimental table was positioned directly in front of the participants, with a pressure button located in close proximity to the participants and two grip force sensors placed slightly further away. Before the

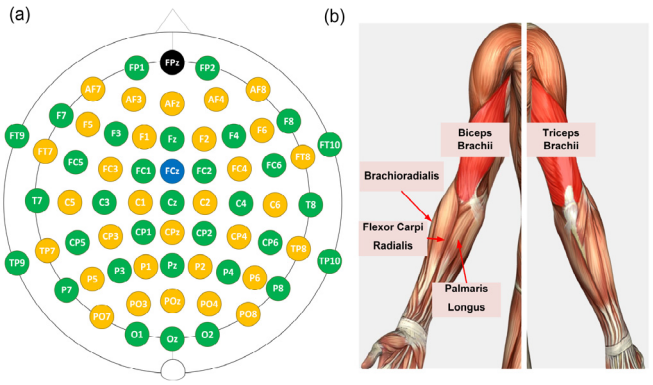

Fig. 1. Data Acquisition Scheme. (a) EEG Electrodes Set Up. (b) sEMG Electrodes Set up.

experiment, participants sat comfortably in an armchair at an appropriate distance from the experimental table, ensuring that they could naturally reach and grasp the force sensors. In order to record the starting and ending of their movements, participants were required to place their right hands on the pressure button (see Fig. 2a). During the experiment, participants were instructed to complete 5 natural reach-and-grasp tasks according to the auditory cue (see Fig. 2b). Our experimental paradigm was shown as Fig. 2c. Each trial consisted of three stages: preparation, execution, and rest, with a duration of 12 seconds per trial.

1) Preparation stage: At second 0, an auditory cue indicated a specific task, such as "medium wrap" or "adducted thumb", and participants should maintain a resting gesture without any movement.

2) Execution stage: At second 2, an auditory beep was generated. During this stage, participants naturally extended their right hand towards the grip force sensor, performed the task action and maintained it for a period of time before retracting their hand back to the pressure button.

3) Rest stage: An auditory cue of "please rest" was given. During this stage, participants can blink, swallow, relax, and wait for the next trial.

During the experiment, participants were required to avoid blinking, swallowing, and other body movements except during the rest stage.

In total, the experiment consisted of 10 runs, with each run comprising 30 trials. Therefore, 300 trials were obtained for each participant. During each run, the sequence of the five natural grasp tasks was randomized, but their frequencies were equal. To prevent muscle fatigue, participants were provided with a rest period of 5 to 10 minutes after each run. Before the experiment, participants participated in a practice run to acquaint themselves with the experimental procedure.

C. Data Acquisition

We used a 64-channel ActiCAP electrode cap (ActiCAP Systems, Brain Products GmbH, Germany) for EEG recording. The electrode placement adhered to the international 10-20 system (see Fig. 1a). The FCz channel served as the reference channel, while the FPz channel was used as the ground channel. To attenuate the high-frequency components, a bandpass Butterworth filter with a range of 0.01 to 100Hz was applied. Additionally, a 50Hz notch filter was utilized to reduce power line interference. During the experiment, the sampling rate was set at 1000Hz and electrode impedances were kept below 15kΩ.

In addition, we employed Trigno TM wireless EMG devices (DelsysInc, Natick, MA, USA) to capture sEMGs from five muscles (see Fig. 2b), including biceps brachii (BB), triceps brachii (TB), brachioradialis (BR), flexor carpi radialis (FCR), and palmaris longus (PL). Additionally, a 4-channel USB3102A data acquisition card was adopted to record the output of the pressure button, synchronous trigger and grip force sensors. The sampling frequency of both sEMG and data acquisition card was 2000Hz.

D. Movement Moment Detection

To investigate the EEG changes during different movement stages, we utilized the rising and falling edges of the pressure button to detect the movement onset and end of each trial. Additionally, the initiation and termination of participants' grasping actions were determined based on the corresponding rising and falling edges of the grip force sensor signal. During this step, trials that satisfied any one of the four criteria listed below were excluded: 1) the participant reached out before the beep prompt; 2) the participant did not return to the button within 5 seconds after the beep prompt; 3) the participant's reaction time exceeded 2 seconds; 4) the participant performed an incorrect action.

E. Signal Preprocessing

Signals in this study were preprocessed using BrainVision Analyzer 2.2 and MATLAB R2021b (Mathworks, Inc., USA).

Firstly, EEG was re-referencing to the average of TP9 and TP10 channels, which were located at mastoids. Next, the re-referenced EEG was filtered from 0.01 to 45Hz using a zero-phase fourth-order Butterworth bandpass filter. We set Fp1 channel as ocular reference channel, and applied independent component analysis (ICA) [33] to remove ocular components. Finally, using the beep cue moment as the reference (0s), a time range of $[-2, 4.9]$s was extracted as the time region of interest (tROI) and baseline correction was performed by $[-2, 0]$s.

For sEMG, the first step was to align the sEMG signals with the force data using the rising edge of the synchronous trigger. Since the duration of one run was 6 minutes and the sampling rates of both force data and sEMG data were 2000Hz, the length of the force data and sEMG data for a run was 720000 samples. By using the rising edge of the synchronous trigger signal, the starting point of the data alignment can be determined, achieving data synchronization.

After alignment, sEMG was downsampled to 1000Hz to align with the EEG. Then, the sEMG was mean-centered to remove the DC component. We filtered the mean-centered data from 0.5 to 200 Hz with a zero-phase fourth-order Butterworth bandpass filter. After that, a 50Hz notch filter was utilized to eliminate high-frequency components and power line interference.

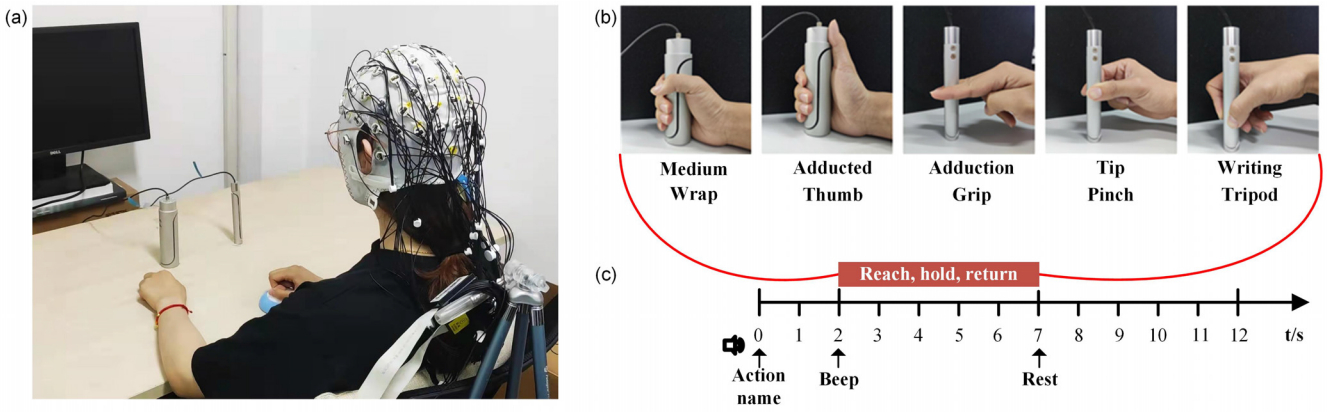

Fig. 2. Natural Reach-and-Grasp Experiment. (a) The Experimental Table. (b) Grasping Tasks. (c) Audio-Cued Experimental Paradigm.

Finally, the preprocessed EEG and sEMG were bandpass filtered by fourth-order zero-phase Butterworth filter to obtain corresponding MRCP (0.1-3Hz), δ (0.5-4Hz), θ (4-8Hz), α (8-13Hz), β (13-30Hz) and γ (30-45Hz) components.

F. EEG Source Estimation

Due to the volume conduction effect, EEG has a relatively low spatial resolution. To overcome this limitation, we employed EEG source imaging techniques to project the scalp EEG ($\boldsymbol{x}$) onto the cortical surface ($\boldsymbol{s}$, current densities of sources):

$$\boldsymbol{x} = \boldsymbol{L}\boldsymbol{s} + \boldsymbol{n} \tag{1}$$

where $\boldsymbol{L}$ represents the lead field matrix determined by the head model and the positions of EEG electrodes and $\boldsymbol{n}$ represents the noise matrix. In this study, we used the 0.5-s rest stage data to estimate $\boldsymbol{n}$ and applied weighted minimum norm estimation (wMNE) to compute $\boldsymbol{L}$ [34]:

$$\min_{\boldsymbol{s}} \boldsymbol{L}\boldsymbol{s} - \boldsymbol{x}_2^2 + \lambda \boldsymbol{W}\boldsymbol{s}_2^2 \tag{2}$$

where λ denotes the regularization parameter, and $\boldsymbol{W}$ represents the weighted matrix.

Finally, we obtained the estimated source $\hat{\boldsymbol{s}}$:

$$\hat{\boldsymbol{s}} = \boldsymbol{L}^T \left(\boldsymbol{L}\boldsymbol{L}^T + \lambda \boldsymbol{W}\right)^{-1} \boldsymbol{x} \tag{3}$$

Currently, among several EEG source imaging methods, the most commonly used one is sLORETA. sLORETA is a generalization of wMNE based on the standardized assumption of current density, with higher positioning accuracy than wMNE. Therefore, in our research, we use sLORETA as the method for solving the inverse problem of source imaging.

The EEG source estimation was realized with Brainstorm toolbox [35]. Colin 27 average brain template was chosen due to its high signal-to-noise ratio and well-defined structure. To minimize errors caused by the head model, we warped the template according to standard electrode position of the EEG cap. After that, we utilized OpenMEEG [36] for solving the forward problem and sLORETA [37] for addressing the inverse problem.

Due to the large number of dipoles calculated by the ESI method, we divided 68 cortical regions of interest (cROI) based on the Desikan-Killiany cortical atlas [38] and averaged the dipoles in the same region to obtain an average source signal, which was referred to as "source EEG" in the following analysis.

G. Feature Extraction and Classification

The feature extraction and classification in this study serves two purposes. Firstly, to determine whether the source signals of MRCP (sMRCP) can differentiate between different types of grasps. Secondly, to assess whether it is possible to identify the subtle distinction within the same grasp type.

To reduce computational load, the sMRCP were downsampled to 100Hz. We used a time window of 100ms for feature extraction. Within this window, the amplitudes of all sMRCP were sampled every 20ms, which allowed for the extraction of 6×68 features.

Given the high dimensionality of the features, we utilized the minimum Redundancy Maximum Relevance (mRMR) criterion [39] to select the most representative 25 features for classifier training and testing. Besides, considering the small sample size characteristic of the EEG data, the shrinkage linear discriminant analysis (sLDA) classifier [40] was employed in this study for grasp type decoding, and 5-fold cross-validations were repeated 10 times to calculate the classification accuracy. The time window slid along tROI with a step size of 10ms, resulting in a total of 681 classification models over the whole tROI.

H. Coupling Analysis

Inter-muscular coupling reflects the interaction between muscles, while cortical-muscular coupling reflects the functional connectivity between brain intention and muscle response. In this study, we focused on source EEG and preprocessed sEMG, evaluating the inter-muscular coupling strength and cortical-muscular coupling strength using coherence analysis and Granger causality analysis, respectively. Especially, during cortical-muscular analysis, we put more attention on source EEG of precentral and postcentral regions, since they respectively contained the primary motor cortex and the primary somatosensory cortex [41], [42].

For a pair of signals $x(t)$ and $y(t)$, their coherence can be described using the cross-power spectral density:

$$C_{xy}(f) = \frac{S_{xy}(f)}{\sqrt{S_{xx}(f)S_{yy}(f)}} \tag{4}$$

In the equation (4), $S_{xy}(f)$ represents the cross-power spectral density between the two signals, $S_{xx}(f)$ and $S_{yy}(f)$ indicate the self-power spectral densities of the two signals, respectively.

However, traditional coherence analysis is unable to capture the causal relationship between the cerebral cortex and muscles, which is not conducive to our investigation into the cortical-muscular response mechanisms. To address this limitation, we employed Granger causality analysis:

$$G_{y\to x} = \ln \frac{S_{xx}(f)}{\mathrm{H}_{xx}(f)\Sigma\mathrm{H}^*_{xx}(f)} \tag{5}$$

Equation (5) represents the Granger causality relationship from y(t) to x(t), where $S_{xx}(f)$ represents the self-power spectral density of $x(t)$, $\mathrm{H}_{xx}(f)$ denotes the transfer matrix, and Σ represents the covariance matrix.

The above calculation was realized using Brainstorm toolbox. Besides, to verify the significance of the coupling index, we calculated the credible threshold of the coupling index based on the reference [43]:

$$\mathrm{CL} = 1 - (1-\alpha)^{\frac{1}{N-1}} \tag{6}$$

where N represents the number of trials, and α represents the confidence level, which was set to 0.95 in our study. Only coherence values and Granger causality values greater than CL were considered significant. To quantitatively describe the differences in inter-muscular coupling and cortical-muscular coupling under different frequency bands, we further defined the significant area. Taking coherence values as an example:

$$S = \sum_f \begin{cases} \Delta f \times \left(C_{xy}(f) - CL\right) & \text{if } C_{xy}(f) > CL \\ 0 & \text{otherwise} \end{cases} \tag{7}$$

where Δf represents the frequency resolution. A larger value of S indicates a stronger coupling strength within this frequency band.

III. Results

A. Behavioral Analysis

Fig. 3 shows the movement behavioral analysis for all participants. From Fig. 3a, it could be observed that the total time of the movement varies among different participants, while the reaction time remains similar. The average reaction time for each grasping task across all participants was calculated, and a one-way analysis of variance (ANOVA) was also conducted (see Fig. 3b). Bonferroni post-hoc tests demonstrated that there were no significant differences in reaction time among different grasping actions ($p > 0.05$).

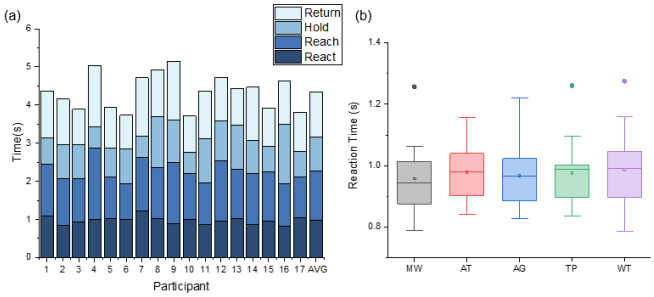

Fig. 3. Movement behavioral analysis of all participants. 0s indicates the beep prompt moment. The circle point indicates the outliers. (a) Movement stage for each participant in a trial. (b) Reaction time of all participants across different grasping tasks.

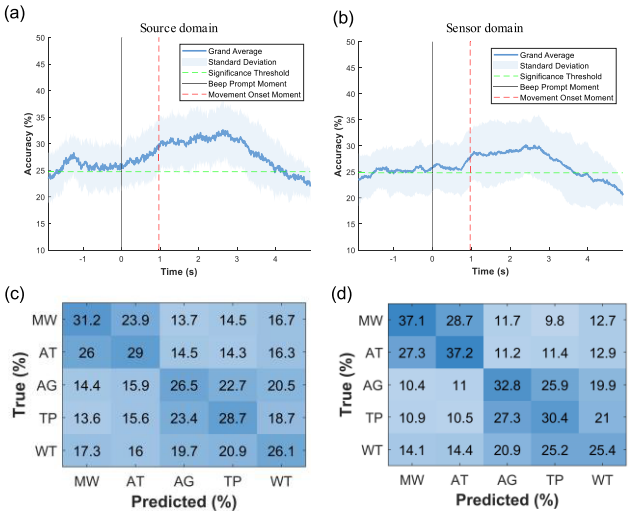

Fig. 4. Five-class classification results. (a) Grand average classification accuracy source domain over tROI. Significance threshold is 24.74% ($\alpha = 0.05$). (b) Grand average classification accuracy of sensor domain over tROI. Significance threshold is 24.74% ($\alpha = 0.05$). (c) Grand average row-normalized confusion matrix at −1.24s. (d) Grand average row-normalized confusion matrix at 2.63s.

B. Multiclass Classification Results

Fig. 4 presents the grand average five-class classification results of grasp types. Since the small sample size of the EEG may lead to a random classification level of more than 20% for five-class classification, we calibrated the chance level of the classification results based on [44], and [45]. The grand average significance level for the five-class classification is 24.74% ($\alpha = 0.05$). Fig. 4a and Fig. 4b illustrate the grand average accuracy of source and sensor domain over the whole tROI. The peak accuracy of the source domain is 32.6%, and the peak accuracy of the sensor domain is 30.1%. It can be seen that the accuracy of the source domain is slightly higher than that of the sensor domain.

Specifically, for the source domain, the classification accuracy gradually increases at the beginning of tROI, and reaches a peak of 32.6% during the hold stage. After that, the accuracy curve gradually declines to the vicinity of the significance level. In addition, as shown in Fig. 4a, there are two peaks in the accuracy curve, located before and after the beep prompt (0s), respectively. According to previous literature [9]

TABLE I
PARTICIPANT-SPECIFIC PEAK PERFORMANCE AND THEIR CORRESPONDING TIME POINT (MULTICLASS CLASSIFICATION)

Participant	Before		After		
	Time (s)	Acc (%)	Time (s)	Acc (%)	Stage
S1	-1.11	30.4	1.53	36.6	Reach
S2	-1.43	30.3	0.97	34.7	Reach
S3	-1.00	32.4	1.97	37.9	Reach
S4	-1.59	28.1	3.30	37.1	Hold
S5	-1.24	26.2	2.73	37.2	Hold
S6	-1.47	29.8	2.14	32.2	Hold
S7	-1.57	43.8	1.79	50.0	Reach
S8	-0.07	31.8	0.75	39.4	React
S9	-1.11	32.5	2.88	37.3	Hold
S10	-1.42	27.4	2.68	37.4	Hold
S11	-0.16	32.1	2.61	32.8	Hold
S12	-0.49	36.2	3.20	44.8	Hold
S13	-1.44	34.1	3.49	41.1	Hold
S14	-1.23	31.4	2.83	36.1	Hold
S15	-1.32	29.6	2.46	42.4	Hold
S16	-0.83	34.6	0.24	37.9	React
S17	-1.28	28.1	2.02	40.7	Reach
AVG.	/	31.7	/	38.6	/
Grand Avg.	-1.24	27.6	2.63	32.6	Hold

and our speculation, the reason for the first peak may be the participant's intention to move.

Table I displays the two peak performances for all participants. Most participants realized their peak decoding performance in the hold phase or late stage of the reach phase. Besides, since inconsistent time taken by each participant to achieve peak performance, the grand average peak performance (32.6%) is 6% lower than average peak performance (38.6%).

Fig. 4c and Fig. 4d display the grand average row-normalized confusion matrices corresponding to two peak time points. It can be observed that sMRCP can effectively distinguish between power grasp and precision grasp, but it is difficult to differentiate between actions belonging to the same grasping type.

Furthermore, we conducted binary classification studies between power grasp (MW and AT) and precision grasp (TP and WT), as well as between MW and AT within the power grasp category. The grand average binary classification accuracy curve for power grasp and precision grasp is shown in Fig. 5. The grand average binary classification accuracy for power grasp versus precision grasp is above the significance level (56.03%, $\alpha = 0.05$) throughout the whole tROI, with a peak accuracy of 70.0%. Participant-specific peak performance of binary classification is displayed in Table II. The average binary classification accuracy difference of the two studies reaches 12.2%.

C. Coherence Analysis

To investigate the relationship between intermuscular coupling strength and frequency, we divided the tROI into 7 windows and calculated the coherence of sEMG signals for each muscle pair within 1-second interval, as shown in Fig. 6. In the figure, only four muscle pairs, which is PL-FCR, FCR-BR, TB-BB, and PL-BR, exhibited strong coherence above the significance threshold. Moreover, there is a clear

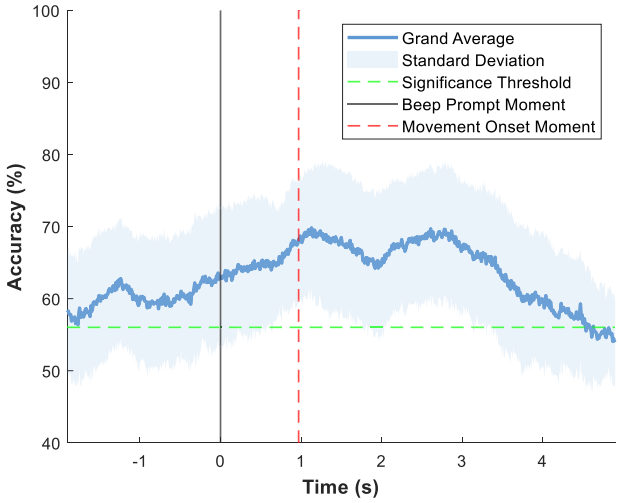

Fig. 5. Binary classification results over tROI. Grand average classification accuracy between power grasps and precision grasps.

TABLE II
PARTICIPANT-SPECIFIC PEAK PERFORMANCE AND THEIR CORRESPONDING TIME POINT (BINARY CLASSIFICATION)

Participant	Power vs. Precision		MW vs. AT		Difference
	Time (s)	Acc (%)	Time (s)	Acc (%)	
S1	1.42	73.3	1.53	67.0	6.3
S2	0.87	80.8	3.61	66.5	14.3
S3	2.77	70.0	2.03	63.8	6.2
S4	2.96	81.4	0.28	61.3	20.1
S5	2.76	71.9	4.86	62.3	9.6
S6	2.21	71.3	0.96	61.7	9.6
S7	2.06	99.8	4.02	72.4	27.4
S8	0.87	87.3	2.12	68.5	18.8
S9	3.26	72.3	1.53	61.3	11.0
S10	2.36	77.0	2.47	59.3	17.7
S11	0.02	72.0	2.45	70.8	1.2
S12	3.40	80.4	0.82	72.9	7.6
S13	3.22	86.1	1.78	64.5	21.6
S14	2.48	80.6	2.70	63.8	16.8
S15	1.08	77.6	2.41	70.2	7.5
S16	0.88	74.1	1.26	70.6	3.6
S17	1.30	81.4	2.55	73.3	8.1
AVG.	/	78.7	/	66.5	12.2
Sig.		51.6		52.2	-0.6

trend indicating that higher frequencies correspond to greater coherence. Additionally, time interval between [1, 4]s exhibited the highest intermuscular coherence, which aligns with the movement execution stage.

In Fig. 7, the grand average coherence areas of different frequency bands are displayed. It can be observed that intermuscular coupling is most visible in the high-frequency bands, and each frequency band's coupling strength is ranked as follows: $\gamma > \beta > \alpha \approx \delta > \theta$. Among them, the highest coupling strength of δ frequency band is observed during the preparation stage, while the highest coupling strengths of other frequency bands occur during the execution stage. Besides, the strongest coupling of γ and β frequency band is observed between the PL and FCR as well as between the FCR and BR during the holding phase, and the strongest coupling in the α frequency band is observed between the TB and BB during the reaching phase.

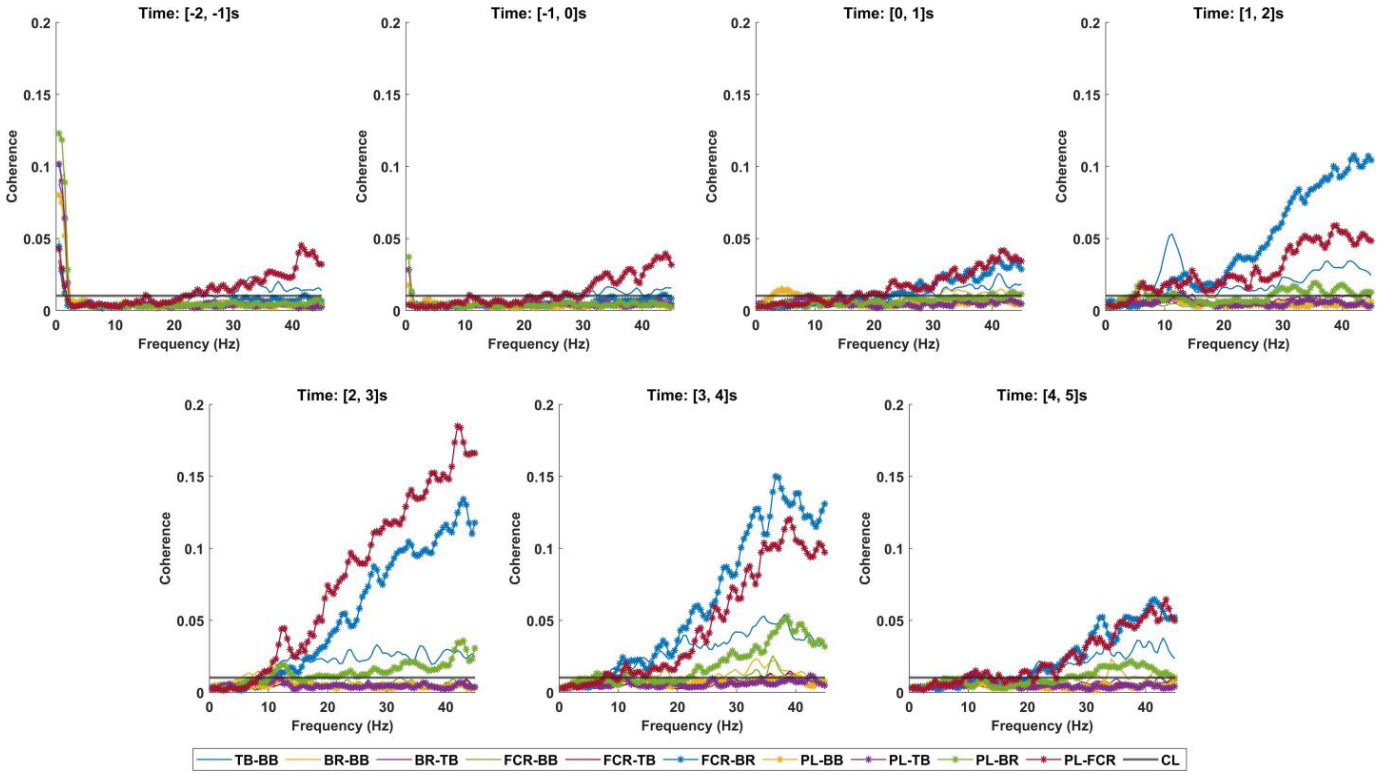

Fig. 6. The grand average intermuscular coherence over frequency in different time intervals.

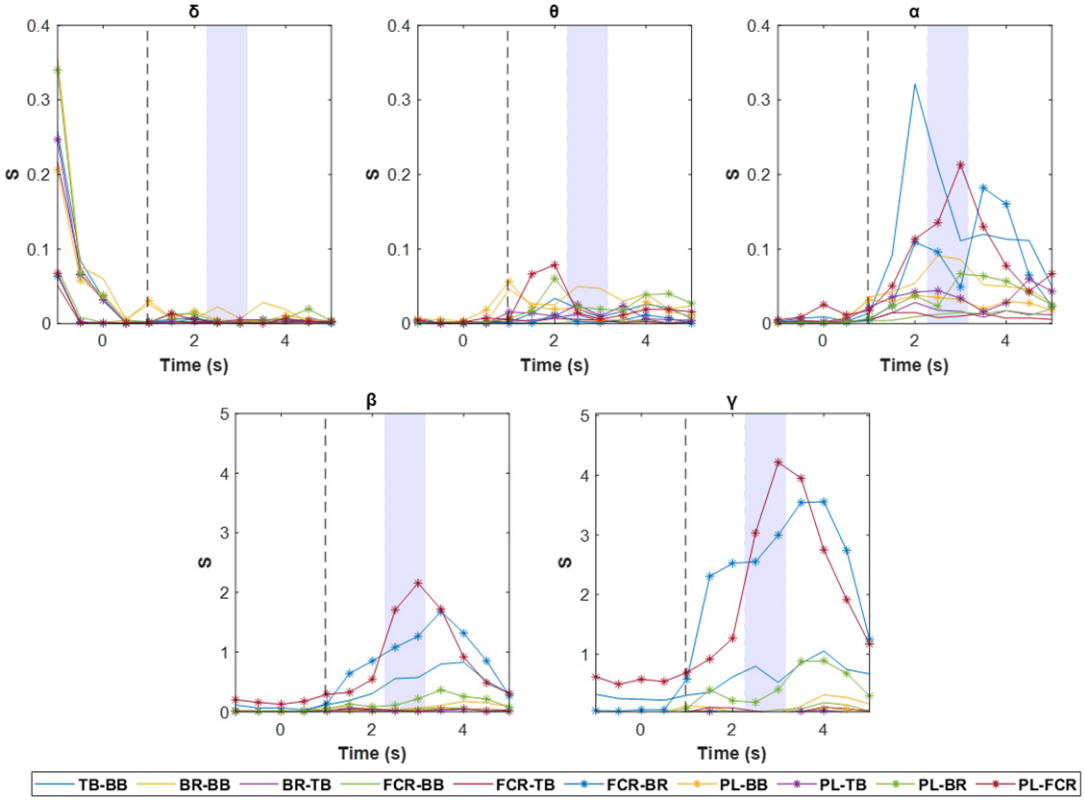

Fig. 7. The grand average coherence areas of different frequency bands. The black vertical dotted line indicates the actual movement onset. The light blue filled area indicates the phase of holding.

Fig. 8 presents the grand average coherence areas of different muscle pairs. From the figure, it can be observed that the trends of coupling strength for various muscle pairs are generally consistent in the β and γ frequency bands, which typically exhibit two peaks. For the upper arm muscle pairs of TB-BB, these two peaks correspond to the late stages of

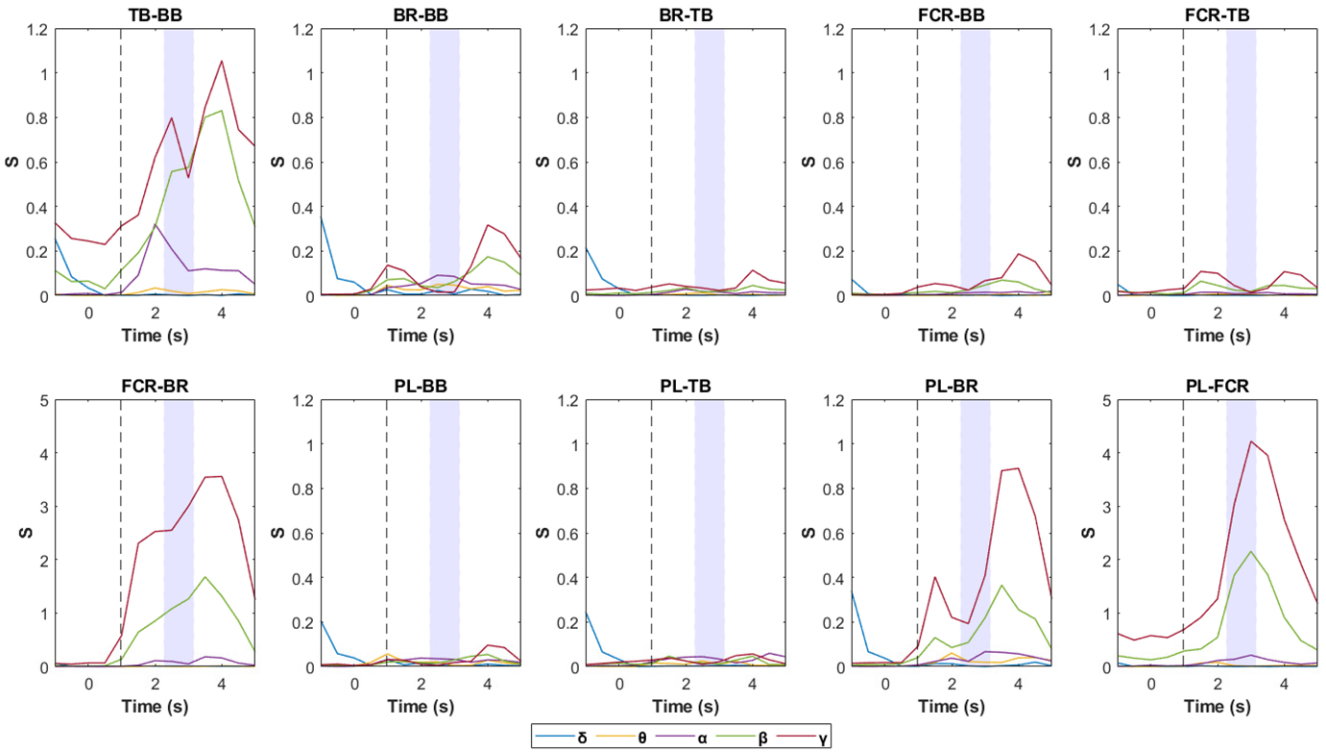

Fig. 8. The grand average coherence areas of different muscle pairs. The black vertical dotted line indicates the actual movement onset. The light blue filled area indicates the phase of holding.

the reaching phase and the grasping phase, respectively, and the latter peak shows slightly higher strength than the former peak. For the lower arm, the two coupling peaks of PL-BR and FCR-BR also occur during the reaching phase and the holding phase. However, compared to PL-BR, the coupling strength of FCR-BR does not show a significant decrease during the grasping phase but maintaining a stable coupling level. Additionally, the coupling strength of PL-FCR begins to increase from the grasping phase and reaches its highest peak at the end of the grasping phase, exhibiting only one peak.

Besides, compared to the non-execution stage, the coupling strength of sEMG signals is higher during the movement execution stage. Additionally, during the preparation stage, the early coupling strength is greater than the late coupling strength. Moreover, the coupling strength during the holding phase is higher than that during the reaching phase.

Fig. 9 and Fig. 10 present the grand average cortical-muscular coupling strength between the both-side source EEG of the postcentral and precentral regions and three muscle channels (BR, FCR, PL) in different directions. Overall, the coupling strength in the upward direction (from sEMG to EEG) is higher than that in the downward direction (from EEG to sEMG). However, the coupling strength in the γ frequency band shows an opposite phenomenon, especially during the preparation and holding phases. It is worth noting that for the downward direction, strong coupling is observed primarily in the γ frequency band, while the coupling strength in other frequency bands remains relatively consistent.

When comparing specific coupling pairs in the upward direction, it is observed that the cortical-muscular coupling strength in the same frequency band shows consistency across different phases. In the δ frequency band, the coupling strength between sEMG and the right source EEG is higher than that between sEMG and the left source EEG. In the θ frequency band, the coupling strength between sEMG and Precentral L is the highest, followed by that with Postcentral R. In the α frequency band, the coupling pattern is opposite to that in the δ frequency band, except during the reaching phase. In the α frequency band, the coupling strength between sEMG and the left source EEG is higher than that between sEMG and the right source EEG. In the β frequency band, the coupling pattern is opposite to the θ frequency band, with higher coupling strength observed between sEMG and Postcentral R compared to the coupling strength between sEMG and Precentral L. Furthermore, in the δ and θ frequency bands, it is noted that the transfer of information between FCR and the cortical regions is slightly higher compared to the other two muscle channels and the brain.

IV. Discussion

In this study, we selected five common natural grasping actions based on grasp taxonomy and investigated the decoding feasibility of MRCP source features. Both binary classification and multiclass classification approaches achieved better-than-chance classification accuracies, with average peak performances of 78.7% (Power vs. Precision), 66.5% (MW vs. AT), and 38.6% (5-class classification), respectively. Moreover, we quantitatively analyzed the temporal variations and frequency band differences of inter-muscular and cortical-muscular coupling strengths during natural grasping process.

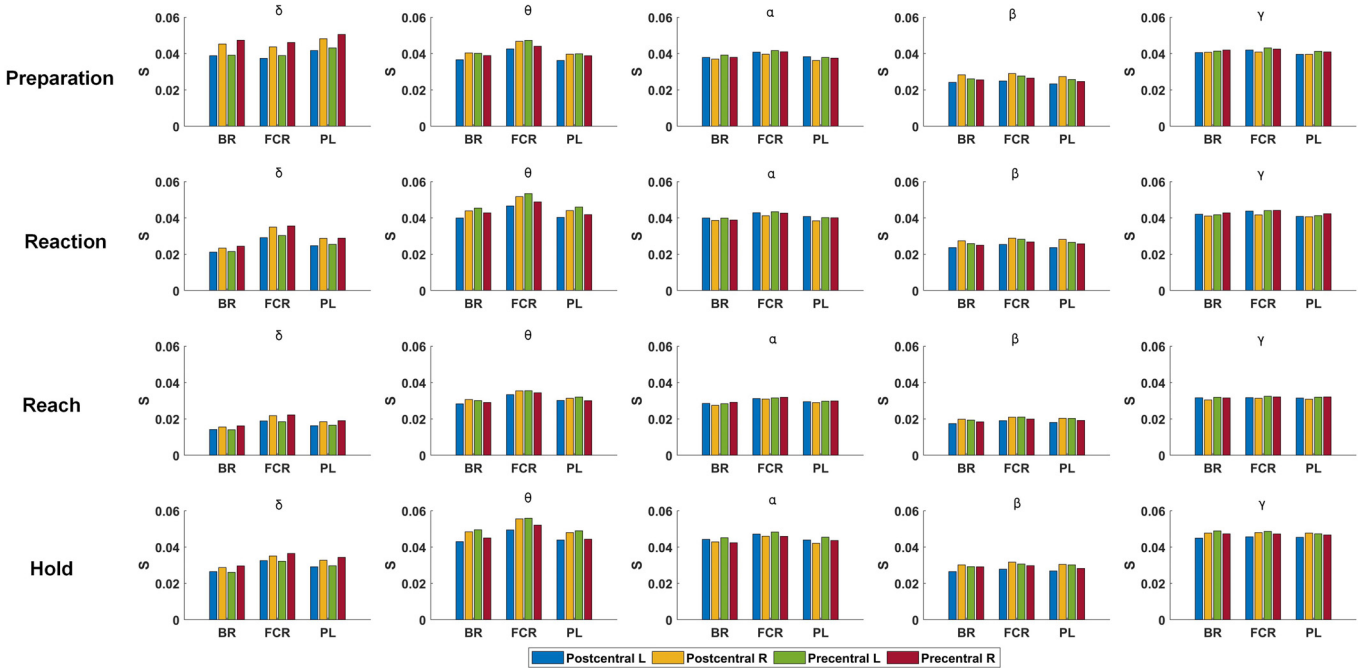

Fig. 9. Grand average significant area of granger causality in the upward direction (from sEMG to EEG).

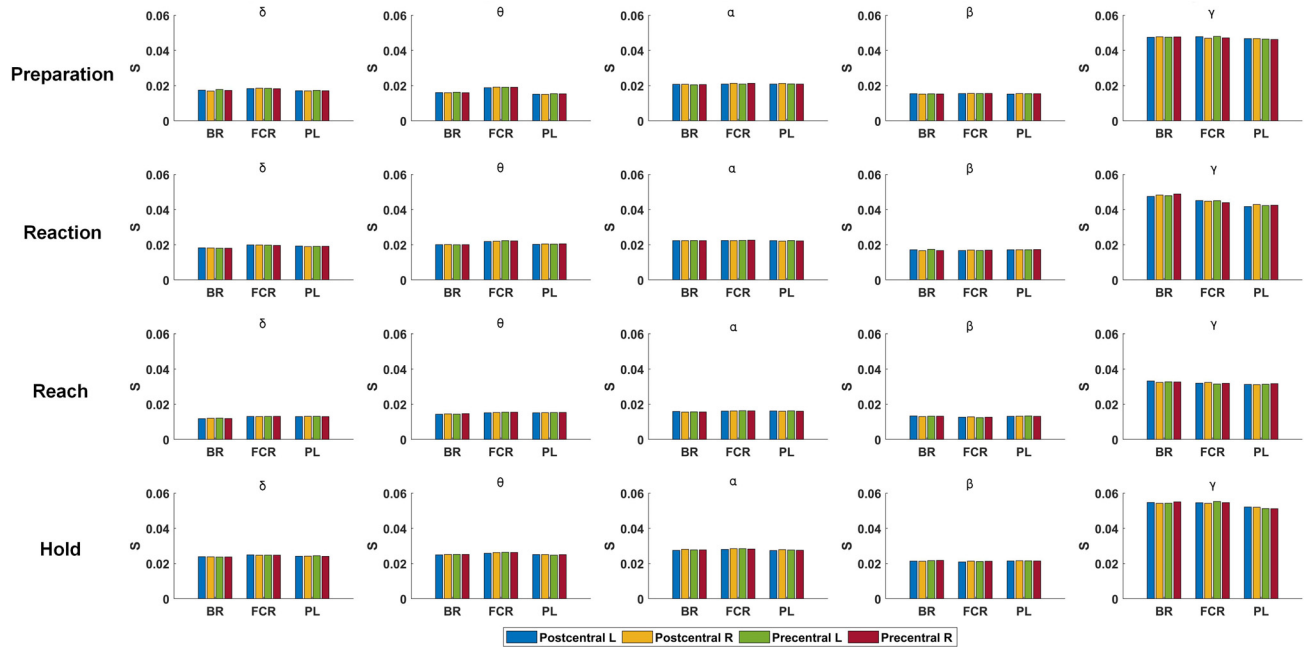

Fig. 10. Grand average significant area of granger causality in the downward direction (from EEG to sEMG).

A. Single Trial Classification

We successfully decoded five natural grasping actions using MRCP source features. However, from the confusion matrices in Fig. 4, it can be observed that source features belonging to different grasp types are not easily confused with each other. Specifically, source features of power grasps such as MW and AT are prone to confusion, while source features of precision grasps such as AG, TP, and WT are likely to be confused with each other. On the contrary, there is less confusion between power grasps and precision grasps. Fig. 5 provides a more intuitive representation of this phenomenon.

On the one hand, this can be attributed to the inherent differences between the actions. From the perspective of grasp taxonomy, grasping actions can generally be classified into two categories [30]: precision grasps and power grasps (some studies categorize them into 3 class, which include intermediate class [31]). Actions within the same category exhibit minimal differences. For instance, the only distinction between MW and AT lies in the abduction of the thumb, making it challenging for sMRCP to discriminate between them effectively. In our experiment, the objects used for power grasps and precision grasps had different diameters.

Previous research suggested that MRCP primarily decoded the properties of the grasped object during the movement observation phase and it can accurately decode the grasp type during whole movement execution phase [7]. This may explain why the classification accuracy for power grasps and precision grasps is higher than the significance level during the preparation stage, whereas MW and AT only reach significant classification levels during the execution stage.

On the other hand, this phenomenon can be explained by the neural control of different grasping actions. Researchers found that precision grasps and power grasps were separate in terms of their neural innervation [46]. Precision hand movements were primarily controlled by the median nerve, which was often referred to as the "precision nerve". Besides, grip force was mainly governed by the ulnar nerve, known as the "power nerve" [47]. Previous studies about hand-related EEG decoding did not take the impact of grasp taxonomy into account. The results of our research reflect the precise movement control provided by the brain's neural pathways when executing different natural grasp types, which offer neurological support for the grasp taxonomy.

Furthermore, in Table I, the peak accuracies for the five-class classification of most participants occur during the hold phase or late stage of the reach phases. This finding was consistent with our previous research [29] and was in line with the results Schwarz et al. obtained in their study [13]. According to the reference [48], [49], the information about hand shape gradually increased as the hand approached the object, reaching its maximum during the holding phase. As a result, the shape distinction in these two phases was the most pronounced, as demonstrated by our results, leading to higher classification accuracy.

B. Inter-Muscular Coupling

The results of our study indicated that the coherence between sEMG signals increases with higher frequencies. However, we also noticed strong coherence between different muscle combinations within the frequency range of 0.5∼2 Hz (see Fig. 6). This phenomenon was observed only during the movement preparation phase ([−2, 0]s) and decreased over time. It is important to highlight that we were unable to locate any prior research indicating that substantial muscle coupling existed during the movement preparation phase. Therefore, it might be challenging to tell whether this strong coherence represents muscle preparation for upcoming actions or is merely the result of artifacts caused by muscle tremor during the rest stage.

Furthermore, we noted a significant peak coherence at 12Hz throughout the execution stage ([1, 4]s). Interestingly, during the transition from the reach phase ([1, 2]s) to the hold phase ([2, 3]s), this peak shifts from the upper arm muscles (TB-BB) to the lower arm muscles (PL-FCR). Combined with the findings of Sburlea et al. [50], which showed that during the holding phase of grasping, contralateral parietal EEG in the μ frequency band indicated muscle activity, we speculated that this peak reflected the transfer of movement information between muscles during planning and execution phase.

Additionally, Li's research demonstrated that there was strong coupling among synergistic muscles, particularly in the γ and β frequency bands [51], which was consistent with our results: in Fig. 7 and Fig. 8, strong coherence in the γ and β frequency bands are observed, specifically between PL-FCR and FCR-BR during the hold phase. Additionally, in the α frequency band, there is a strong coherence between TB and BB. Typically, TB and BB indicated arm movements, while PL, FCR, and BR indicated hand movements. Therefore, we speculated that during natural grasping, finer movement execution information was transmitted in the β and γ frequency band, while movement planning Information was conveyed in in higher frequency bands. Besides, the growing coupling strength over time in Fig. 8 indicated that coupling information accumulated over time.

C. Cortical-Muscular Coupling

The coupling strength between EEG and sEMG varies across different frequency bands because different frequency bands are associated with specific neural mechanisms and functional interactions between the brain and muscles. The results of this study show that, except for the hold phase in the γ band, the coupling strength from sEMG to EEG is higher than the coupling strength from EEG to sEMG, reflecting the differences in direction-synchronized oscillations between sensory feedback and motor control mechanisms, which is in line with the findings of Zhu's research [25]. Additionally, prior study revealed that γ band oscillations were intimately tied to cognitive functioning and related to shifts in attention [52]. During the transition from movement preparation to execution, the participants' attention was enhanced, accompanied by increased activities in the γ frequency band. Higher levels of downward coupling strength in the γ frequency band during the hold phase were the outcome of this increased activity because it supported the sensory cognition's selective attentional processes.

Besides, it is noteworthy that for the downward direction, the cortical-muscular coupling strength within the same movement phase and frequency band is nearly identical. However, there are noticeable variations in the upward direction. This finding implies that while the precise feedback information connected to the execution of movements differs across various muscle groups, the amount of control information transmitted from the brain to the muscles remains constant.

Furthermore, in this study, we found that the reach phase exhibited the lowest coupling strength compared to other phases, regardless of frequency band and direction. The peculiar features of the reach phase may be responsible for this discovery. During reach phase, participants engage in dynamic movements, the limb movements introduced interference, leading to a decrease in the analysis of coupling strength. In contrast, the hold phase demonstrated the highest cortical-muscular coupling strength among all phases. This can be attributed to two factors. On the one hand, participants keep a static position throughout the holding phase, which prevents interference in signal acquisition. On the other hand, the hold phase demands accurate movement execution and

control, demanding prompt communication between the brain and muscles to ensure the actions are carried out as intended.

D. Limitations and Future Work

In this study, we successfully decoded five natural grasping actions based on MRCP source features, and investigated the inter-muscular coupling and cortical-muscular coupling relationship, opening up new opportunities for natural and refined neural prosthetics and rehabilitation robot control. Based on our findings, further investigations should be considered as follows:

Firstly, our experiment focused only on different types of grasping actions. However, decoding grasping speed and force is equally crucial in real-world situations. Therefore, future studies could consider incorporating movement parameter control in the experimental design.

Secondly, our study employed offline decoding strategy. Future study could focus on online decoding and device control for brain-muscle fusion, enabling real-time applications, even if the efficiency of online analysis was considered throughout the feature extraction and classification process by using smaller time windows (100ms) for decoding.

Additionally, our study primarily concentrated on extracting the source amplitude features of MRCP. Future research could concentrate on extracting features from both time domain and frequency domain to improve decoding precision. Deep learning techniques may also be incorporated into the analysis to enhance the decoding performance. These methods might help us gain a more thorough understanding of the brain correlates and make it possible to decode motor-related information from EEG signals more precisely.

Lastly, it should be highlighted that the physiological signals collected in this study were from healthy participants. However, patients with SCI or disabilities may show unusual physiological patterns in their EEG and sEMG. Therefore, even if it is difficult, it is vitally necessary to confirm the reliability and precision of our findings on SCI participants.

V. Conclusion

In this study, we employed MRCP source features to decode complicated grasping actions and investigated the temporal changes and frequency band differences in inter-muscular coupling and cortical-muscular coupling strength during the movement process. Both multi-classification and binary classification results showed that MRCP source features could effectively distinguish between power grasp and precision grasp. Furthermore, we observed peaks in inter-muscular coupling strength whose frequency similar to the μ rhythm in the EEG. Our research helps BCIs be controlled naturally and intuitively and has significant ramifications for our comprehension of the control and feedback systems underlying human hand grasping performance.

References

[1] J. R. Wolpaw et al., "Brain-computer interface technology: A review of the first international meeting," *IEEE Trans. Rehabil. Eng.*, vol. 8, no. 2, pp. 164–173, Jun. 2000.

[2] G. Pfurtscheller, G. R. Müller, J. Pfurtscheller, H. J. Gerner, and R. Rupp, "'Thought'—Control of functional electrical stimulation to restore hand grasp in a patient with tetraplegia," *Neurosci. Lett.*, vol. 351, no. 1, pp. 33–36, Nov. 2003.

[3] M. Rohm et al., "Hybrid brain–computer interfaces and hybrid neuroprostheses for restoration of upper limb functions in individuals with high-level spinal cord injury," *Artif. Intell. Med.*, vol. 59, no. 2, pp. 133–142, Oct. 2013.

[4] A. Shakeel, M. S. Navid, M. N. Anwar, S. Mazhar, M. Jochumsen, and I. K. Niazi, "A review of techniques for detection of movement intention using movement-related cortical potentials," *Comput. Math. Methods Med.*, vol. 2015, pp. 1–13, Oct. 2015.

[5] P. Ofner, A. Schwarz, J. Pereira, and G. R. Müller-Putz, "Upper limb movements can be decoded from the time-domain of low-frequency EEG," *PLoS ONE*, vol. 12, no. 8, Aug. 2017, Art. no. e0182578.

[6] P. Ofner, A. Schwarz, J. Pereira, D. Wyss, R. Wildburger, and G. R. Müller-Putz, "Attempted arm and hand movements can be decoded from low-frequency EEG from persons with spinal cord injury," *Sci. Rep.*, vol. 9, no. 1, p. 7134, May 2019.

[7] A. I. Sburlea, M. Wilding, and G. R. Müller-Putz, "Disentangling human grasping type from the object's intrinsic properties using low-frequency EEG signals," *Neuroimage: Rep.*, vol. 1, no. 2, Jun. 2021, Art. no. 100012.

[8] K. Wang, M. Xu, S. Zhang, Y. Ke, and D. Ming, "Analysis and classification for EEG patterns of force motor imagery using movement related cortical potentials," in *Proc. 40th Annu. Int. Conf. IEEE Eng. Med. Biol. Soc. (EMBC)*, Jul. 2018, pp. 211–214.

[9] J. Pereira, P. Ofner, A. Schwarz, A. I. Sburlea, and G. R. Müller-Putz, "EEG neural correlates of goal-directed movement intention," *NeuroImage*, vol. 149, pp. 129–140, Apr. 2017.

[10] G. R. Müller-Putz et al., "Decoding of continuous movement attempt in 2-dimensions from non-invasive low frequency brain signals," in *Proc. 10th Int. IEEE/EMBS Conf. Neural Eng. (NER)*, May 2021, pp. 322–325.

[11] M. Zhang et al., "Decoding coordinated directions of bimanual movements from EEG signals," *IEEE Trans. Neural Syst. Rehabil. Eng.*, vol. 31, pp. 248–259, 2023.

[12] M. Jochumsen, I. K. Niazi, D. Taylor, D. Farina, and K. Dremstrup, "Detecting and classifying movement-related cortical potentials associated with hand movements in healthy subjects and stroke patients from single-electrode, single-trial EEG," *J. Neural Eng.*, vol. 12, no. 5, Oct. 2015, Art. no. 056013.

[13] A. Schwarz, P. Ofner, J. Pereira, A. I. Sburlea, and G. R. Müller-Putz, "Decoding natural reach-and-grasp actions from human EEG," *J. Neural Eng.*, vol. 15, no. 1, Feb. 2018, Art. no. 016005.

[14] K. Wang, M. Xu, Y. Wang, S. Zhang, L. Chen, and D. Ming, "Enhance decoding of pre-movement EEG patterns for brain–computer interfaces," *J. Neural Eng.*, vol. 17, no. 1, Jan. 2020, Art. no. 016033.

[15] J. Wang, L. Bi, A. G. Feleke, and W. Fei, "MRCPs-and-ERS/D-oscillations-driven deep learning models for decoding unimanual and bimanual movements," *IEEE Trans. Neural Syst. Rehabil. Eng.*, vol. 31, pp. 1384–1393, 2023.

[16] S. Asadzadeh, T. Y. Rezaii, S. Beheshti, A. Delpak, and S. Meshgini, "A systematic review of EEG source localization techniques and their applications on diagnosis of brain abnormalities," *J. Neurosci. Methods*, vol. 339, Jun. 2020, Art. no. 108740.

[17] N. Srisrisawang and G. R. Müller-Putz, "Applying dimensionality reduction techniques in source-space electroencephalography via template and magnetic resonance imaging-derived head models to continuously decode hand trajectories," *Frontiers Hum. Neurosci.*, vol. 16, p. 137, Mar. 2022.

[18] V. S. Handiru, A. P. Vinod, and C. Guan, "EEG source space analysis of the supervised factor analytic approach for the classification of multi-directional arm movement," *J. Neural Eng.*, vol. 14, no. 4, Aug. 2017, Art. no. 046008.

[19] Y. Hou, L. Zhou, S. Jia, and X. Lun, "A novel approach of decoding EEG four-class motor imagery tasks via scout ESI and CNN," *J. Neural Eng.*, vol. 17, no. 1, Feb. 2020, Art. no. 016048.

[20] R. J. Kobler, E. Kolesnichenko, A. I. Sburlea, and G. R. Müller-Putz, "Distinct cortical networks for hand movement initiation and directional processing: An EEG study," *NeuroImage*, vol. 220, Oct. 2020, Art. no. 117076.

[21] C. Li, H. Guan, Z. Huang, W. Chen, J. Li, and S. Zhang, "Improving movement-related cortical potential detection at the EEG source domain," in *Proc. 10th Int. IEEE/EMBS Conf. Neural Eng. (NER)*, May 2021, pp. 214–217.

[22] J. Gross, P. A. Tass, S. Salenius, R. Hari, H. Freund, and A. Schnitzler, "Cortico-muscular synchronization during isometric muscle contraction in humans as revealed by magnetoencephalography," *J. Physiol.*, vol. 527, no. 3, pp. 623–631, Sep. 2000.

[23] C. L. Witham, C. N. Riddle, M. R. Baker, and S. N. Baker, "Contributions of descending and ascending pathways to corticomuscular coherence in humans," *J. Physiol.*, vol. 589, no. 15, pp. 3789–3800, Aug. 2011.

[24] W. Omlor, L. Patino, M.-C. Hepp-Reymond, and R. Kristeva, "Gamma-range corticomuscular coherence during dynamic force output," *NeuroImage*, vol. 34, no. 3, pp. 1191–1198, Feb. 2007.

[25] F. Zhu, Y. Li, Z. Shi, and W. Shi, "TV-NARX and coiflets WPT based time-frequency Granger causality with application to corticomuscular coupling in hand-grasping," *Frontiers Neurosci.*, vol. 16, Sep. 2022, Art. no. 1014495.

[26] L. Zhou et al., "Cortico-muscular coherence of time–frequency and spatial characteristics under movement observation, movement execution, and movement imagery," *Cognit. Neurodynamics*, to be published.

[27] B. Xu et al., "Decoding different reach-and-grasp movements using non-invasive electroencephalogram," *Frontiers Neurosci.*, vol. 15, Sep. 2021, Art. no. 684547.

[28] B. Xu et al., "Decoding hand movement types and kinematic information from electroencephalogram," *IEEE Trans. Neural Syst. Rehabil. Eng.*, vol. 29, pp. 1744–1755, 2021.

[29] B. Xu et al., "Electroencephalogram source imaging and brain network based natural grasps decoding," *Frontiers Neurosci.*, vol. 15, Nov. 2021, Art. no. 797990.

[30] Y. Yang, C. Fermüller, Y. Li, and Y. Aloimonos, "Grasp type revisited: A modern perspective on a classical feature for vision," in *Proc. IEEE Conf. Comput. Vis. Pattern Recognit. (CVPR)*, Jun. 2015, pp. 400–408.

[31] T. Feix, J. Romero, H.-B. Schmiedmayer, A. M. Dollar, and D. Kragic, "The GRASP taxonomy of human grasp types," *IEEE Trans. Human-Mach. Syst.*, vol. 46, no. 1, pp. 66–77, Feb. 2016.

[32] I. M. Bullock, J. Z. Zheng, S. De La Rosa, C. Guertler, and A. M. Dollar, "Grasp frequency and usage in daily household and machine shop tasks," *IEEE Trans. Haptics*, vol. 6, no. 3, pp. 296–308, Jul. 2013.

[33] T.-W. Lee, M. Girolami, and T. J. Sejnowski, "Independent component analysis using an extended infomax algorithm for mixed subgaussian and supergaussian sources," *Neural Comput.*, vol. 11, no. 2, pp. 417–441, Feb. 1999.

[34] S. Iwaki and S. Ueno, "Weighted minimum-norm source estimation of magnetoencephalography utilizing the temporal information of the measured data," *J. Appl. Phys.*, vol. 83, no. 11, pp. 6441–6443, Jun. 1998.

[35] F. Tadel, S. Baillet, J. C. Mosher, D. Pantazis, and R. M. Leahy, "Brainstorm: A user-friendly application for MEG/EEG analysis," *Comput. Intell. Neurosci.*, vol. 2011, pp. 1–13, Jan. 2011.

[36] A. Gramfort, T. Papadopoulo, E. Olivi, and M. Clerc, "OpenMEEG: Opensource software for quasistatic bioelectromagnetics," *Biomed. Eng. OnLine*, vol. 9, no. 1, p. 45, 2010.

[37] R. D. Pascual-Marqui, "Standardized low-resolution brain electromagnetic tomography (sLORETA): Technical details," *Methods Findings Exp. Clin. Pharmacol.*, vol. 24, pp. 5–12, Feb. 2002.

[38] R. S. Desikan et al., "An automated labeling system for subdividing the human cerebral cortex on MRI scans into gyral based regions of interest," *NeuroImage*, vol. 31, no. 3, pp. 968–980, Jul. 2006.

[39] H. Peng, F. Long, and C. Ding, "Feature selection based on mutual information criteria of max-dependency, max-relevance, and min-redundancy," *IEEE Trans. Pattern Anal. Mach. Intell.*, vol. 27, no. 8, pp. 1226–1238, Aug. 2005.

[40] B. Blankertz, S. Lemm, M. Treder, S. Haufe, and K.-R. Müller, "Single-trial analysis and classification of ERP components—A tutorial," *NeuroImage*, vol. 56, no. 2, pp. 814–825, May 2011.

[41] L. Banker and P. Tadi, *Neuroanatomy, Precentral Gyrus*. Treasure Island, FI, USA: StatPearls Pub, 2022. [Online]. Available: http://europepmc.org/books/NBK544218

[42] E. Kropf, S. K. Syan, L. Minuzzi, and B. N. Frey, "From anatomy to function: The role of the somatosensory cortex in emotional regulation," *Brazilian J. Psychiatry*, vol. 41, no. 3, pp. 261–269, May 2019.

[43] D. M. Halliday, J. R. Rosenberg, A. M. Amjad, P. Breeze, B. A. Conway, and S. F. Farmer, "A framework for the analysis of mixed time series/point process data—Theory and application to the study of physiological tremor, single motor unit discharges and electromyograms," *Prog. Biophys. Mol. Biol.*, vol. 64, nos. 2–3, pp. 237–278, 1995.

[44] G. Müller-Putz, R. Scherer, C. Brunner, R. Leeb, and G. Pfurtscheller, "Better than random: A closer look on BCI results," *Int. J. Bioelectromagn.*, vol. 10, no. 1, pp. 52–55, 2008.

[45] E. Combrisson and K. Jerbi, "Exceeding chance level by chance: The caveat of theoretical chance levels in brain signal classification and statistical assessment of decoding accuracy," *J. Neurosci. Methods*, vol. 250, pp. 126–136, Jul. 2015.

[46] J. R. Napier and R. H. Tuttle, *Hands*, vol. 9. Princeton, NJ, USA: Princeton Univ. Press, 1993.

[47] H. Kesserwani, "Pseudo-anterior interosseus nerve syndrome: A case report and a review of clinical signs, pathology and functional anatomy of the precision grip," *Cureus*, vol. 13, May 2021, Art. no. e15180.

[48] L. S. Jakobson and M. A. Goodale, "Factors affecting higher-order movement planning: A kinematic analysis of human prehension," *Exp. Brain Res.*, vol. 86, no. 1, pp. 199–208, Aug. 1991.

[49] U. Castiello, "The neuroscience of grasping," *Nature Rev. Neurosci.*, vol. 6, no. 9, pp. 726–736, Sep. 2005.

[50] A. I. Sburlea and G. R. Müller-Putz, "Exploring representations of human grasping in neural, muscle and kinematic signals," *Sci. Rep.*, vol. 8, no. 1, Nov. 2018, Art. no. 16669.

[51] X. Li, Y. Du, C. Yang, W. Qi, and P. Xie, "Merging of synergistic muscles and intermuscular coherence predict muscle coordination complexity," in *Proc. IEEE Int. Conf. Inf. Autom. (ICIA)*, Aug. 2016, pp. 791–795.

[52] C. Liu et al., "Modulating gamma oscillations promotes brain connectivity to improve cognitive impairment," *Cerebral Cortex*, vol. 32, no. 12, pp. 2644–2656, Jun. 2022.